Jurnal Penelitian Fisika dan Aplikasinya (JPFA)
Volume 12, Issue 2, December 2022
https://journal.unesa.ac.id/index.php/jpfa/

p-ISSN: 2087-9946
e-ISSN: 2477-1775

Implementation of the Poisson Impedance Inversion to Improve Hydrocarbon Reservoir Characterisation in the Poseidon Field, Browse Basin, Australia

Riky Tri Hartagung [a] and Mohammad Syamsu Rosid [b,*]

Department of Physics, Faculty of Mathematics and Sciences, Universitas Indonesia
Depok 16424, Indonesia

E-mail: [a] rikytri10@gmail.com and [b] syamsu.rosid@ui.ac.id
* Corresponding Author

Received: 24 July 2022; Revised: 20 August 2022; Accepted: 23 September 2022

Abstract

*The prediction process of lithology and fluid content is the most important part of reservoir characterization. One of the methods used in this process is simultaneous seismic inversion. In the Poseidon field, Browse Basin, Australia, the parameters generated through simultaneous seismic inversion cannot accurately characterize the reservoir because of the overlapping impedance values between hydrocarbon sand, water sand, and shale, which cause a high level of ambiguity in the interpretation. The Poisson impedance (PI) inversion provides a solution to this problem by rotating the impedance a few degrees through coefficient c. Coefficient c is obtained through the target correlation coefficient analysis by finding the optimum correlation coefficient between the PI and the target log, namely, gamma rays, effective porosity, and resistivity. The results show that the PI gives better outcomes in separating hydrocarbon-saturated reservoir zones. Based on the results of the lithology impedance–gamma rays, the ϕI-effective porosity cross-plot, and the fluid impedance-water saturation (Sw) cross-plot, with optimum correlations of 0.74, 0.91, and 0.82, respectively. The lithology of hydrocarbon-saturated porous sand is at values of LI $\leq$ 2800 (m/s)(g*cc), ϕI $\leq$ 5500 (m/s)(g*cc) and FI $\leq$ 4000 (m/s)(g*cc). The presence of low values for LI, ϕI and FI correlates accurately with the presence of hydrocarbons in the well. Each value of c is then applied to the seismic data. The results show that this method can determine the distribution of gas-saturated porous sand on the seismic inversion section in the northeast–southwest direction.*

Keywords: *Reservoir characterisation; Poisson impedance; Browse Basin; Poseidon field*

How to cite: Hartagung R T and Rosid M S. Implementation of the Poisson Impedance Inversion to Improve Hydrocarbon Reservoir Characterisation in the Poseidon Field, Browse Basin, Australia. *Jurnal Penelitian Fisika dan Aplikasinya (JPFA)*. 2022; **12**(2): 102–114.

INTRODUCTION

The Browse Basin in Western Australia stretches in a northeast–southwest direction and potentially contains hydrocarbon sources and reserves [1]. Based on geochemical data, the main potential source of hydrocarbons in the Browse Basin is in the Plover Formation, which has a fluvio–deltaic sandstone lithology covered by siltstone and claystone, dated between the Early to Middle Jurassic ages [2]. However, the Plover Formation was extended in the Early Jurassic Age, which resulted in faults and anticline collapse in the Triassic Age, so the hydrocarbon reservoirs did not fully accumulate in the Early Jurassic Age [3]. This caused the distribution of the hydrocarbon reservoir to be uncertain because it has changed from the beginning. Therefore, to determine the exact distribution of the hydrocarbon reservoir, it is necessary to carry out a reservoir characterization process.

Reservoir characterization is a qualitative and quantitative prediction process of lithology and fluid content done by integrating log, seismic and surface geological data [4]. The reservoir characterization analysis in the Poseidon field was carried out using the *Lambda* over *Mu* (λ/μ) attribute and showed that this attribute could determine the reservoir distribution [5]. However, Quakenbush et al. [6] state that, mathematically, the λ/μ attribute does not consider the discrimination caused by density (*rho*) because it can be transformed into ($V_P{}^2/V_S{}^2 - 2$). This is similar to the Poisson ratio, which cannot distinguish between gas sand and oil sand. The characterization of the Poseidon reservoir has been conducted using acoustic and multi-attribute impedance [7]. The results show that this method can only discover the distribution of the reservoir but not the fluid content. This is because the acoustic impedance (AI) alone is not sufficient to predict the porosity and fluid content properties, due to the overlapping lithology (sandstone/shale) and fluid content [8]. Therefore, other attributes are needed to improve the reservoir characterization.

Many approaches and studies have been carried out to characterize reservoirs more accurately. One of them is the Poisson impedance (*PI*). Quakenbush et al. [6] used the PI attribute in the Norwegian North Sea and achieved the best results in determining reservoir boundaries. Direzza et al. [9] applied this attribute to characterize the reservoir in the Talang Akar Formation by separating the lithology of sandstone from shale, and they achieved good results in identifying the fluid content. Rosid et al. [8] also implemented the attribute to characterize the sandstone reservoir in the Talang Akar Formation. The results show that this attribute can separate lithology from shale and hydrocarbons from water as well as determine the fluid content in the reservoir and the thickness of the hydrocarbon reservoir.

Based on the analysis of the dataset used in this study, the Poseidon field reservoir area has a low Poisson's ratio value and density. The PI attribute is effectively used for all reservoirs where the Poisson's ratio and density values are low or high anomaly [6]. The values of the (*AI*) and the shear impedance (*SI*) in this data also overlap with each other due to the presence of shale inserts that fill the rock pores, causing ambiguity in determining their limits [10]. The PI is a solution to the difficulties in separating the lithology-fluid distribution on the x and y axes in the cross-plot between the *AI* and *SI* with a rotation factor (*c*) [11].

The *AI* and *SI* values used herein were obtained using the simultaneous seismic inversion method. This method is based on the creation of a low-frequency model [12]. Using the *AI* and *SI* logs, low-frequency models could be created and updated iteratively so that the smallest errors were obtained for the gathered seismic data [13]. Mathematically, the *PI* can be written using the following formula:

$$PI = AI - cSI. \tag{1}$$

The rotation factor (*c*) determines the success of getting the right PI value. The right *PI* value can provide lithological discrimination that is more sensitive than other attributes [14]. Quakenbush et al. [6] first determined the rotation factor (*c*) used in the *PI* attribute by decreasing the Poisson ratio. Zhou et al. [15] determined the rotation factor by approximating the value of the *AI*/*SI* ratio in brine-saturated rocks. However, in this study, the target correlation coefficient analysis (TCCA) [8, 16] was used and refined by adding the correlation with the porosity log because it gave the best results [17]. By analyzing the results of the PI attribute in the form of the lithology impedance (*LI*), the porosity impedance (ϕI) and the fluid impedance (*FI*), the characterization of reservoirs in the Poseidon field, Browse Basin, Western Australia, is expected to improve.

METHOD

This research is a case study that processes geophysical data (seismic data and well log data) from the open-source, TerraNubis, to determine the distribution of hydrocarbon-saturated sandstone. The Poseidon field seismic data used in this study are surface geology, offshore seismic 3D data and well log data, as shown in Tables 1 and 2**.**

Table 1. Angle stack seismic data.

Seismic Data	Angle
Near Stack	0^{o}–12^{o}
Mid Stack	12^{o}–24^{o}
Far Stack	24^{o}–36^{o}

Table 2. Well log data.

Log Data	Kronos	Poseidon 1	Poseidon 2
GR	√	√	√
Caliper	-	√	-
RHOB	√	√	√
NPHI	√	√	√
RD	√	-	√
Vp	√	√	√
Vs	√	√	√
CS	√	√	√
Marker	√	√	√

Wavelet Extraction

The seismic prestack wavelets are affected by the incident angle, so it is necessary to extract wavelets for each partial stack [18]. The simultaneous inversion, processed by the Hampson Russel 10 software, and the wavelet used reflect composite wavelets extracted from the stack angle seismic data. The results of the wavelet extraction of each angle stack can be seen in Figure 1.

Pre-inversion Analysis

Pre-inversion analysis needs to be done before the inversion process is carried out so that the inversion results produced are following the well data. The results of this analysis affect how well the correlation will be between the log data of the low-frequency model and the inversion results for each well [19]. A good correlation provides more accurate inversion results [20]. When the correlation is low and the error is still high, an inversion analysis is carried out, such as initial modeling, wavelet selection or inversion parameters [19]. The results of the pre-inversion analysis can be seen in Figure 2. The red curve shows the inversion yield curve, the blue curve shows the log curve and the black curve shows the initial model curve, which has a synthetic seismogram correlation value with seismic data of 0.979 and an error of 0.204.

Simultaneous inversion is conducted to get the volume of the *AI* and *SI*. These parameters are interpreted and derived into the PI inversion in the form of the *LI*, the *FI* and the ϕI. The inversion uses the optimum value of coefficient *c*, so it can improve the characterization of the hydrocarbon reservoir. The value of coefficient *c* is determined using the TCCA method [17]. The variation of the coefficient *c* value depends on the angle used to calculate the log *PI*.

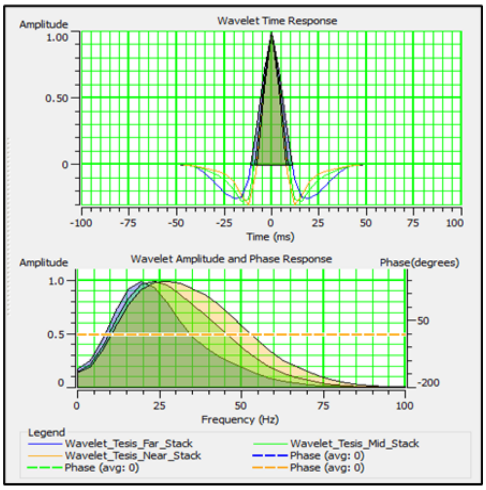

Figure 1. Combined wavelet extraction results on the angle stack seismic data.

The determination of coefficient *c* is established through the correlation of the log *PI* value to target the log that has the optimum correlation. It determines the *LI* log value, which is sensitive to lithology, the ϕI log value, which is sensitive to effective porosity and the *FI* log value, which is sensitive to fluid content. The target logs that are sensitive to lithology are gamma rays (GR), *V*p/*V*s and *Mu-Rho*. The target log that is sensitive to porosity is the NPHI log, and the target logs that are sensitive to fluid content are logs of water saturation, resistivity and Lambda-Rho [21]. The steps taken to obtain the optimum *c* value in the log *PI* can be seen in Figure 3.

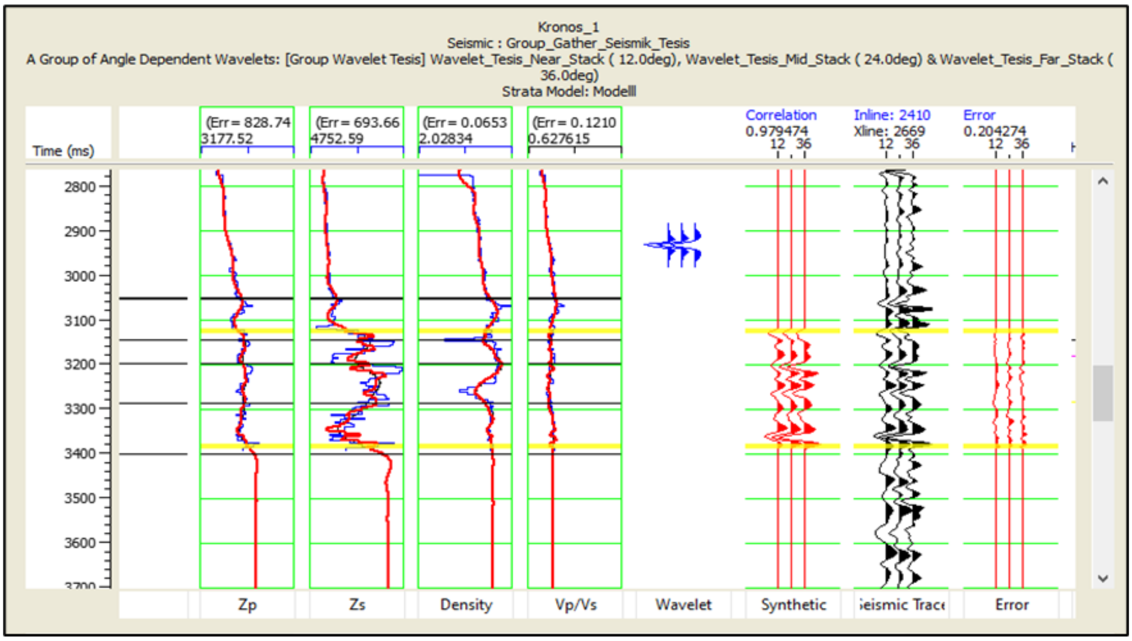

Figure 2. Correlation of synthetic seismograms with seismic data.

The determination of the optimum *c* value to obtain the *LI* logs is limited to the research target, namely the top horizon boundary of the Plover Formation to its base, to obtain a cut-off value between sand and non-sand (shale). The calculation of the ϕI is carried out on the area that is interpreted as sand in the previous stage of the log *LI* calculation. This stage is conducted to separate tight sand and porous sand. The porous sand obtained in the calculation of the log ϕI is used to obtain the optimum *c* value for calculating the *FI* value.

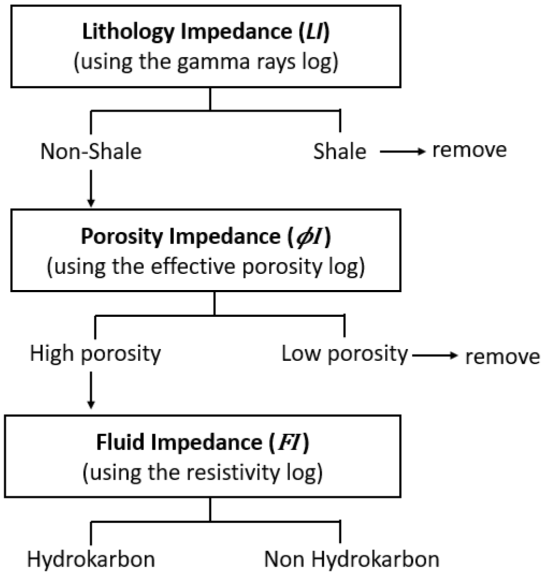

Figure 3. Workflow analysis of the Poisson impedance.

RESULTS AND DISCUSSION

Sensitivity Analysis

The cross-plot analysis between the *AI* and *SI*, shown in Figure 4, shows that the sandstone zone represented in yellow has relatively higher *AI* and *SI* values than the shale zone, which is represented in green. The results show that it is still not possible to separate reservoir and non-reservoir zones because there is overlapping data, which reduces the accuracy of the inversion results.

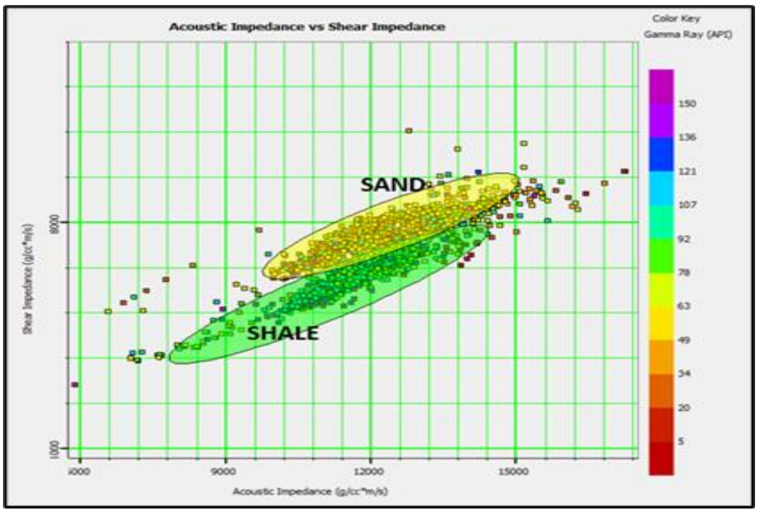

Figure 4. Cross-plot of the acoustic impedance and the shear impedance.

Simultaneous Seismic Inversion

Sensitivity analysis shows that the presence of sandstone and shale lithology produces overlapping values. For this reason, the seismic data slicing is conducted on each parameter resulting from simultaneous inversion. The slicing was done at a time window of 20 ms above the base horizon of the Plover Formation, which was identified as a reservoir in the three wells, as shown in Figure 5. From the *AI* and *SI* inversion distribution maps, it is very difficult to determine the distribution of the reservoir of hydrocarbon-saturated sandstone with shale. This is because the value of the *AI* does not only depend on the type of lithology but also the fluid content [22].

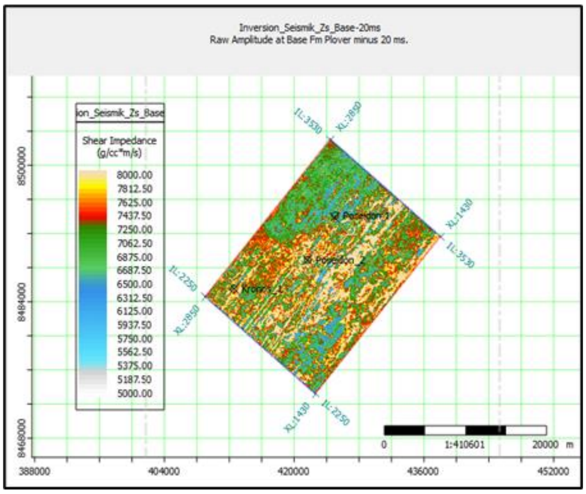

Figure 5. Distribution map of the acoustic impedance and shear impedance inversion over a 20 ms base reservoir.

Target Correlation Coefficient Analysis

The correlation coefficient of the log *PI* with several target logs achieved a good correlation value. This is indicated by the obtained correlation coefficient value that was greater than 0.6 [23]. The optimum correlation between the log *PI* and log GR is obtained when *c* is 2.04, with a correlation of 0.74. The optimum correlation between the log ϕI and log effective porosity is obtained when *c* is 2.28, with a correlation of 0.91. Moreover, the optimum correlation between the log *FI* and log water saturation is obtained when *c* is 1.05, with a correlation of 0.82. The correlation curve for the value of *c* is shown in Figure 6.

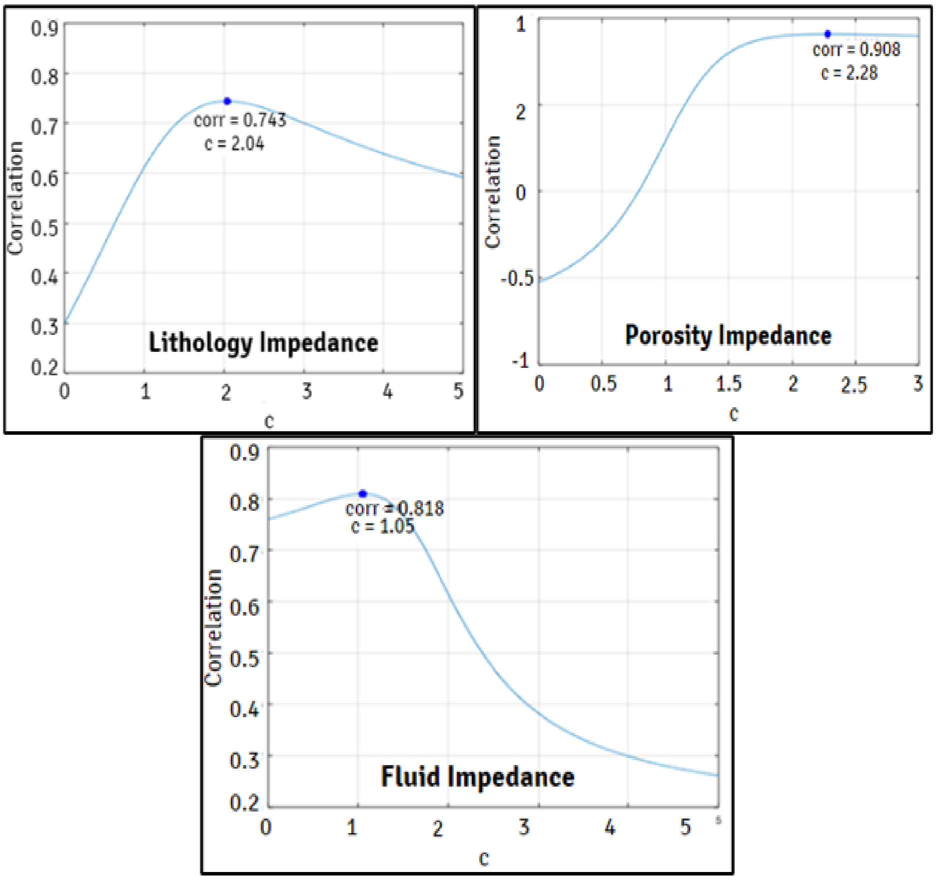

Figure 6. The optimum value to get the Poisson impedance, porosity impedance and fluid impedance logs.

Poisson Impedance

Each coefficient *c* obtained through TCCA is then entered into equation 1, and the equations *LI*, *ϕI,* and *FI* are written as:

$$LI = AI - 2.04SI \tag{2}$$

$$\phi I = AI - 2.28SI \tag{3}$$

$$FI = AI - 1.05SI \tag{4}$$

Then make a cross-plot between the *LI* and *GR*; *ϕI* vs effective porosity, and *FI* vs water saturation, as shown in Figures 7, 8 and 9.

Figure 7 shows the cross-plot between the *LI* and *GR* with the *GR* color bar. From the cross-plot, the *LI* can separate sandstone from shale well. Overall, the lower the *GR* value, the lower the *LI* value. Low *LI* values (≤-2800 (m/s)(g*cc)) and low *GR* values (≤75API) are interpreted as cut-offs for sand. Furthermore, high *LI* values (2800(m/s)(g*cc)) and high *GR* values (>75 API) are interpreted as shale. Before a cross-plot between the *FI* and water saturation is performed, a cross-plot between *ϕI* and effective porosity is performed to eliminate the effects of shale and porosity [24].

Figure 8 shows the cross-plot between *ϕI* and effective porosity and the color bar effective porosity using the sandstone data obtained in the *LI* and *GR* cross-plot. Overall, the value of effective porosity in the sandstone data obtained in the previous cross-plot turned out to be relatively low. This low effective porosity is due to the presence of shale that fills the sandstone and secondary pores that are not connected, so the total porosity is high, and the effective porosity (connected porosity) is low [25]. The quality of the reservoir in this area is very low. From the cross-plot, the *ϕI* can separate tight sandstone from porous sandstone well. Tight sandstone is a sandstone reservoir that has complex porosity and low permeability due to the presence of shale inserts that fill the rock pores [26,27]. Furthermore, porous sandstone is a sandstone reservoir that has a relatively high porosity that is interconnected and permeable [28]. Low *ϕI* values (≤-5500(m/s)(g*cc)) are interpreted as cut-offs for porous sandstone. A high *ϕI* value (> -5500(m/s)(g*cc)) is interpreted as tight sandstone.

When viewed from the cross-section of well *ϕ I*, some data is not highlighted when compared with the cross-section of well *LI*. This indicates that the sandstone interpreted in the *LI* is not completely porous but that some are tight. This tight sandstone is caused by the compaction and cementation process of the shale inserts [29]. Several depths that are not dominantly highlighted in the Kronos well are equal to 4760–4800 m and 4930–4940 m. In the Poseidon 1 well, the depths are equal to 4900–4930 m and 4830–4850 m. In the Poseidon 2 well, the depths are equal to 4980–5030 m.

Figure 9 shows the *FI* and water saturation cross-plot with the water saturation as a color bar. From the cross-plot, the separation between the gas-saturated zone and the water-saturated porous sandstone zone can be observed. The gas-saturated porous sandstone zone has relatively low *FI* and *Sw* (water saturation) values. The value of *Sw* < 0.5 is interpreted as gas-saturated porous sandstone, and *Sw* > 0.5 is interpreted as water-saturated porous sandstone [17]. Viewed from the cross-section of well *FI*, some data is not highlighted when compared with the cross-section of well *ϕI*. This indicates that the porous sandstone interpreted in the *ϕI* is not completely saturated with gas but with water. Low *FI* values (≤ 3750 (m/s)(g*cc)) are interpreted as cut-offs for gas-saturated porous sandstone. Furthermore, a high *FI* value (> 3750 (m/s)(g*cc)) is interpreted as water-saturated porous sandstone. Some of the dominant depths as gas-saturated porous sandstone in the Kronos well are equal to 4998–5037 m; in the Poseidon 1 well, the depths are equal to 4873m–4888 m and 4971–5036 m; in the Poseidon 2 well, the depths are equal to 5084–5092 m and 5261–5281 m.

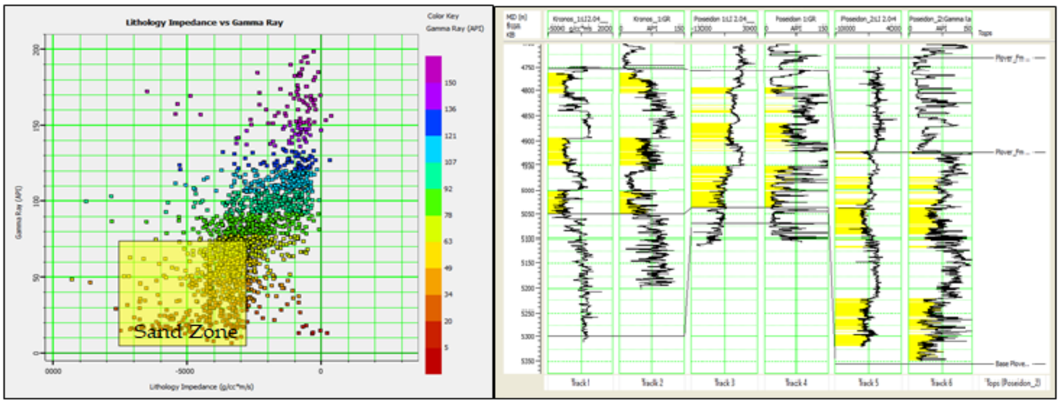

Figure 7. Cross-plot between the lithology impedance and gamma rays with gamma rays as a colour-bar.

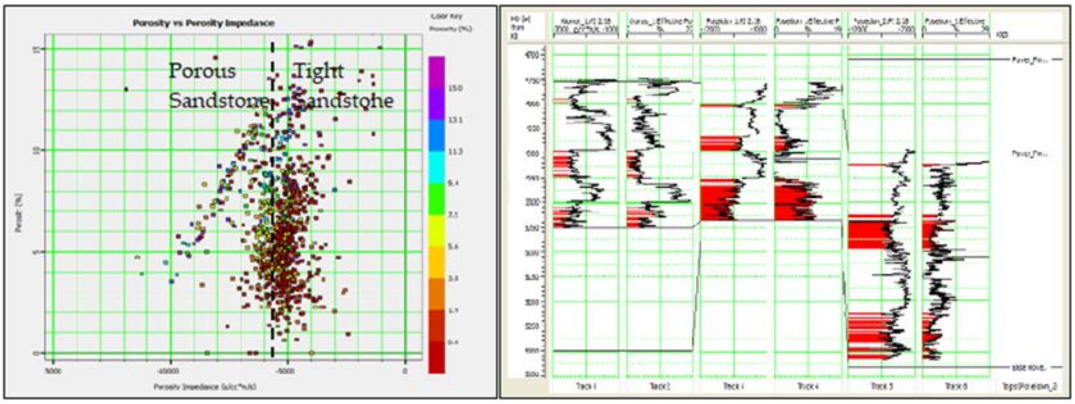

Figure 8. Cross-plot between the porosity impedance and effective porosity with the effective porosity as a colour-bar.

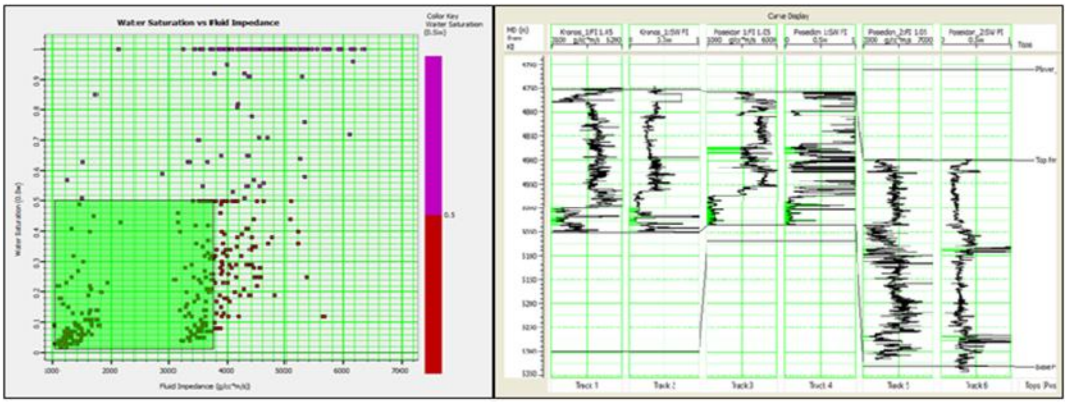

Figure 9. Cross-plot between the fluid impedance and *Sw* with *Sw* as a colour-bar.

Poisson Impedance Inversion

Inversion Analysis of the Lithology Impedance

The slicing process is conducted in a time window of 10 ms to 20 ms below the Plover base horizon, as shown in Figure 10. The area bounded by the yellow line in Figure 10 shows the estimated distribution of sandstone lithology. In the time window 10 ms above the Plover base horizon, the distribution of sandstone lithology appears almost throughout the cross-section, except in the southwest to south. After reaching 20 ms below the Plover base horizon, the sandstone lithology is more widespread than in the previous window. This shows that the distribution area of the sandstone lithology spread from the northwest to the northeast and the south. This slicing shows a better separation than the slicing on the *AI* and *SI* sections.

Inversion Analysis of the Porosity Impedance

To establish the distribution of the sandstone lithology area that has good porosity (porous sandstone), a cross-sectional analysis of the ϕI was carried out with the same time window as the *LI*. Figure 11 shows the ϕI slicing with a time window of 10 ms to 20 ms below the Plover base horizon. The slicing results show some parts of the area that are limited by yellow lines, which were previously interpreted as sandstone lithology and not part of the ϕI. Overall, the west-to-south direction is not limited by a yellow line, so it can be interpreted as tight sandstone. However, in the next slicing time window, a relatively lower value of ϕI begins to appear and spread from the east to the southwest, which is indicated by an area with a yellow line.

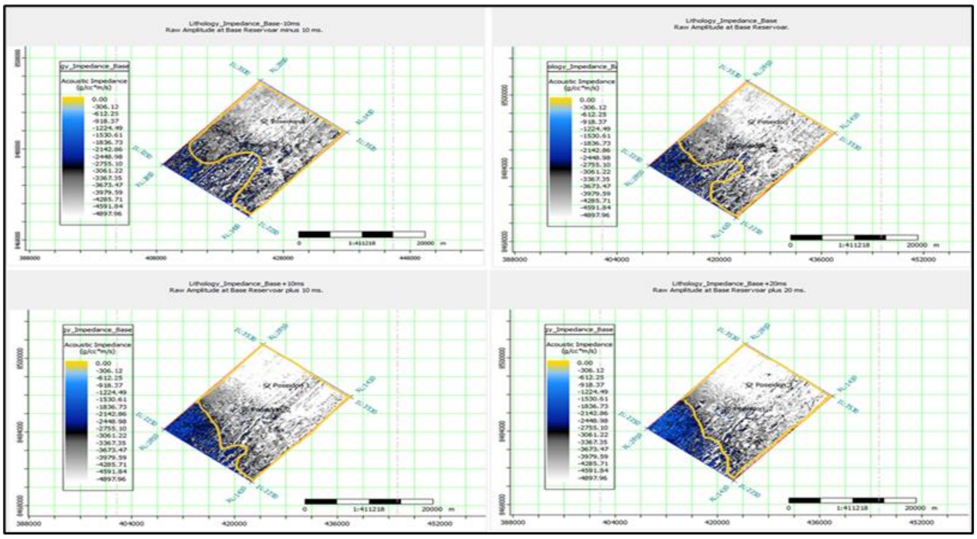

Figure 10. Slicing of the lithology impedance in a 10–20 ms time window upper the Plover base horizon.

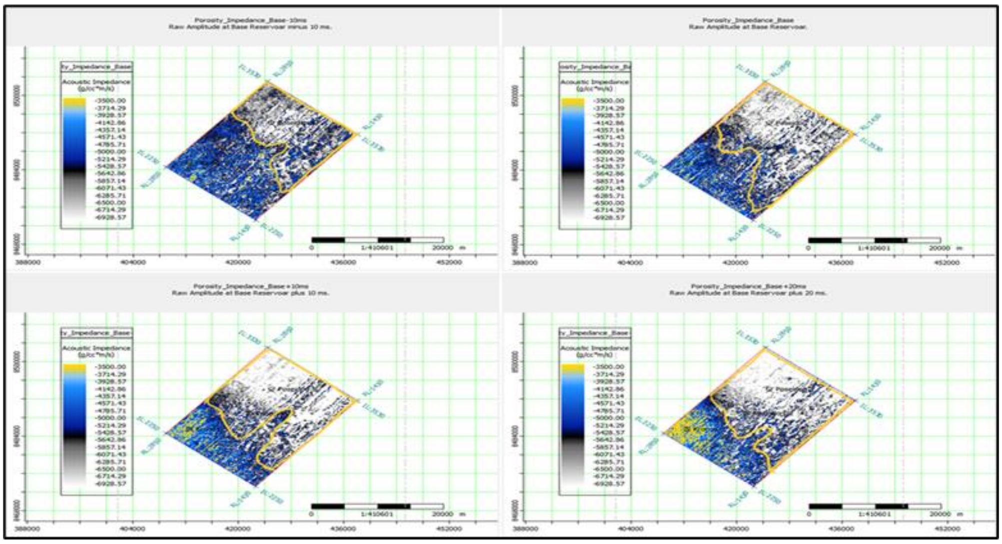

Figure 11. Slicing of the porosity impedance in a 10–20 ms time window upper the Plover base horizon.

Inversion Analysis of Fluid Impedance

The slicing process on the *FI* section is also conducted at the same time window as the *LI* and ϕI, which is 10 ms to 20 ms below the Plover base horizon. The *FI* section can be seen in

Figure 12. The slicing results show several areas that were previously in the ϕI section, which were in the yellow line area and not included in the section in the yellow line area on the *FI* section. This indicates that the area is water-saturated porous sandstone. The fluid content in the form of oil may be in the Montara Formation to the top volcanic while the gas is Plover Formation [2]. This is in accordance with the results of the analysis that states that the area bounded by the yellow line is interpreted as gas-saturated porous sandstone, while in the cross-section, the area is entirely gas.

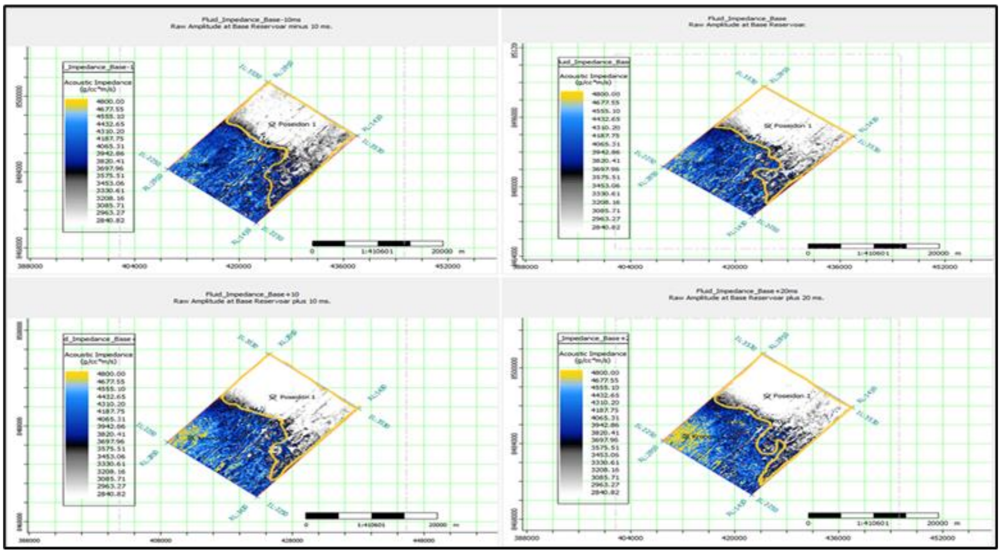

Figure 12. Slicing the fluid impedance in a 10–20 ms time window upper the Plover base horizon.

In contrast with the previous sectional slicing, the *FI* section slicing from 10 ms to 20 ms below the Plover base horizon did not have many significant changes. However, when viewed from the east to the southwest, there are some changes in the presence of gas, which tends to diffuse. These results are based on the use of the rotation factor in the PI formula, which is obtained from the well log correlation. The limitation of this method is that the results of the correlation value with the well log are quite different if there are other wells in an area that has a contrasting lithology that is different from other wells.

From this analysis, it can be said that gas-saturated porous sandstone is dominant in the north to the east area and begins to spread from the east to the south and the southwest. The results of this analysis are verified by Rollet, et al [1] and Adeyosfi [30], which state that the direction of gas distribution is from the northeast to the southwest.

This method can still provide the best results in knowing the distribution of gas-saturated sandstone in the Poseidon field compared with other methods. The PI can be the best solution for all fields to find the distribution of oil–gas sandstone because this method can resolve difficulties in separating the lithology-fluid distribution on the x and y axes in the cross-plot between the *AI* and the *SI* with a rotation factor (c).

CONCLUSION

The PI inversion provides a solution to characterizing the reservoir accurately when the *AI* and the *SI* cannot separate because of the overlapping impedance values between hydrocarbon sand, water sand and shale, which cause a high level of ambiguity in the interpretation by rotating the impedance a few degrees, which is obtained through the coefficient c. The PI inversion can also provide an overview of gas-saturated sandstone lithology with low values of the *LI*, ϕI and *FI*. The distribution of porous sandstone gas saturation in the Plover Formation is from the northeast to the southwest in this study.

AUTHORS' CONTRIBUTION

Riky Tri Hartagung: conceptualization, methodology, data processing and analysis and manuscript drafting. Mohammad Syamsu Rosid: supervision, validation, review, editing and manuscript finalization. All authors have read and agreed to the published version of this manuscript.

STATEMENT OF COMPETITIVE INTEREST

The authors certify that we have no competing financial interests, nor any personal relationship that could influence the work reported in this paper.

REFERENCES

[1] Rollet N, Edwards D, Grosjean E, Palu T, Hall L, Totterdell J, Boreham C, and Murray A. Regional Jurassic sediment depositional architecture, Browse Basin: Implications for petroleum systems. *ASEG Extended Abstracts*. 2018; **2018**(1): 1-8. DOI: https://doi.org/10.1071/ASEG2018abM1_3B.

[2] Conocophillips. *Kronos-1 Well Completion Report Volume 2: interpretation data*. Houston: Conocophillips Company; 2011: 1-954.

[3] Struckmeyer HIM, Blevin JE, Sayers J, Totterdell JM, Baxter K, and Cathro DL. *Structural evolution of the Browse Basin, North West Shelf: new concepts from deep-seismic data.* Beaumaris: Petroleum Exploration Society of Australia (PESA); 2016.

[4] Bosch M, Mukerji T, and Gonzalez EF. Seismic inversion for reservoir properties combining statistical rock physics and geostatistics: A review. *Geophysics*. 2010; **75**(5): 75A165–75A176. DOI: https://doi.org/10.1190/1.3478209.

[5] Sihotang SM. *Identifikasi Persebaran Litologi dan Fluida Hidrokarbon Menggunakan Metode Inversi Seismik Simultan Pada Lapangan Poseidon, Cekungan Browse, Australia*. Undergraduate Thesis. Unpublished. Jakarta: Pertamina University; 2020.

[6] Quakenbush M, Shang B, and Tuttle C. Poisson impedance. *The Leading Edge*. 2006; **25**(2): 128-138. DOI: https://doi.org/10.1190/1.2172301.

[7] Pambudi RR, Mulyatno BS, Sarkowi M, Ramdhani E, Dewanto O, and Wibowo RC. Karakterisasi reservoar dan sumur usulan menggunakan metode seismik inversi acoustic impedance dan multiatribut seismik pada lapangan Poseidon, Australia. *Prosiding Seminar Nasional Ilmu Teknik dan Aplikasi Industri*. 2021; **4**: 128-131. Available from: http://sinta.eng.unila.ac.id/prosiding/index.php/ojs/article/view/36.

[8] Rosid MS, Prasetyo BD, Trivianty J, and Purba H. Characterization of hydrocarbon reservoir at field "B", South Sumatera by using Poisson impedance inversion. *Malaysian Journal of Fundamental and Applied Sciences*. 2019; **15**(3): 472-477. DOI: https://doi.org/10.11113/mjfas.v15n3.1093.

[9] Direzza A and Permana IK. The Application of Poisson Impedance Inversion for Sandstone Reservoir Characterization in the Lower Talang Akar Formation, Case Study Melandong-West Java. *Proceeding of AAPG International Conference & Exhibition*. Singapore: AAPG. 2012. Available from: https://www.searchanddiscovery.com/pdfz/documents/2012/41080direzza/ndx_direzza.pdf.html**?.**

[10] Sørensen MK and Fabricius IL. Clay squirt: Local flow dispersion in shale-bearing sandstones. *Geophysics*. 2017; **82**(1): MR51-MR63. DOI: https://doi.org/10.1190/geo2015-0036.1.

[11] Purba H, Prasetyo BD, Tampubolon RA, Riyadi P, Diria SA, and Basundara AH. Pemisahan litologi dan fluida dengan menggunakan Poisson impedance (Distinguishing Lithology and Fluid Using Poisson Impedance). *Lembaran publikasi minyak dan gas bumi*. 2017; **51**(3): 135-144.
Available from: https://journal.lemigas.esdm.go.id/index.php/LPMGB/article/view/25.

[12] Sumantri I, Haris A, and Riyanto A. Integration of fluid replacement modeling and seismic AVO analysis towards simultaneous seismic inversion to delineate the distribution of Globigerina limestone gas reservoir. *IOP Conference Series: Earth and Environmental Science* 2020; **481**(1): 012051. DOI: https://doi.org/10.17485/IJST/v13i36.770.

[13] Esmaeili S. *Influence of Low Frequencies on Seismic Impedance Inversion.* Master Thesis. Unpublished. Canada: University of Calgary; 2016.

[14] Inyang NJ, Okwueze EE, and Agbasi OE. Detection of gas sands in the Niger Delta by estimation of Poisson's Dampening-Factor (PDF) using wireline log data. *Geosciences*. 2015; **5**(1): 46-51. DOI: https://doi.org/10.5923/j.geo.20150501.06.

[15] Zhou Z and Hilterman FJ. A comparison between methods that discriminate fluid content in unconsolidated sandstone reservoirs. *Geophysics*. 2010; **75**(1): B47-B58. DOI: https://doi.org/10.1190/1.3253153.

[16] Tian L, Zhou D, Lin G, and Jiang L. Reservoir prediction using Poisson impedance in Qinhuangdao, Bohai Sea. *SEG Technical Program Expanded Abstract*. 2010: 2261-2264. DOI: https://doi.org/10.1190/1.3513300.

[17] Kim S, Kim B, Choi J, Byun J, Choi H, and Bang S. Pore fluid estimation using effective workflow of Poisson impedance analysis. *Exploration Geophysics*. 2020; **51**(3): 314-326. DOI: https://doi.org/10.1080/08123985.2019.1690951.

[18] Yu Z, Zhu Z, Wen H, Pan R, and Grenier D. Indicative Factors of Reservoir Sensitivity Based on Pre-stack Inversion. *Journal of Engineering Science & Technology Review*. 2018; **11**(4): 101-110. DOI: https://doi.org/10.25103/jestr.114.13.

[19] Wiyatno OF, Rosid MS, and Purba H. Mapping the Distribution and Characterization of Sandstone Reservoir Using Simultaneous Inversion Method in "OA" Field at Northern Bonaparte Basin. *Journal of Physics: Conference Series*. 2019; **1351(**1): 012045. DOI: http://doi.org/10.1088/1742-6596/1351/1/012045.

[20] Khakhim A. *Pengolahan dan Inversi Poisson Impedance Data Seismik 2D Graben Viking Utara, Laut Utara, Norwegia*. Undergraduate Thesis. Unpublished. Jakarta: Universitas Pertamina; 2020.

[21] Sidiq AP, Manik HM, and Nainggolan TB. Comparative Study of Seismic Migration Method in Characterizing Oil and Gas Reservoirs in Kangean Block, Bali Sea Using Model Based Acoustic Impedance Inversion. *Journal of Tropical Marine Science and Technology*. 2019; **11**(1): 205-219. DOI: http://dx.doi.org/10.29244/jitkt.v11i1.23028.

[22] Maulana T. *Quantitative Seismic Interpretation using Rock Physics Templates-case examples from the Zumba field.* Master Thesis. Norway: Norwegian University of Science and Technology; 2016.

[23] Sugiyono. *Metode Penelitian Kuantitatif, Kualitatif, Dan R&D.* Bandung: Alfabeta; 2017.

[24] Kim S, Lee J, Kim B, and Byun J. Effective workflow of Poisson impedance analysis for identifying oil reservoir with similar resistivity log response to neighboring medias. In *SEG Technical Program Expanded Abstracts 2016*. 2016: 2851-2855. DOI: https://doi.org/10.1190/segam2016-13856496.1.

[25] Pramanik AG, Singh V, Vig R, Srivastava AK, and Tiwary DN. Estimation of effective porosity using geostatistics and multi attribute transforms: A case study. *Geophysics*. 2004; **69**(2): 352-372. DOI: http://dx.doi.org/10.1190/1.1707054.

[26] Liu D, Gu Z, Liang R, Su J, Ren D, Chen B, Huang C, and Yang C. Impacts of pore-throat system on fractal characterization of tight sandstones. *Geofluids*. 2020; **9**: 1-17. DOI: https://doi.org/10.1155/2020/4941501.

[27] Lai J, Wang G, Wang Z, Chen J, Pang X, Wang S, Zhou Z, He Z, Qin Z, and Fan X. A review on pore structure characterization in tight sandstones. *Earth-Science Reviews*. 2018; **177**: 436-457. DOI: https://doi.org/10.1016/j.earscirev.2017.12.003.

[28] Wu H, Zhao J, and Guo N. Multiscale modeling of compaction bands in saturated high-porosity sandstones. *Engineering Geology*. 2019; **261**: 105282. DOI: http://doi.org/10.1016/j.enggeo.2019.105282.

[29] Li B, Zhang H, Xia Q, Peng J, and Guo Q. Quantitative Evaluation of Tight Sandstone Reservoir Based on Diagenetic Facies—A Case of Lower Silurian Kepingtage Formation in Shuntuoguole Low Uplift, Tarim Basin, China. *Frontiers in Earth Science*. 2021; **8**: 597535. DOI: https://doi.org/10.3389/feart.2020.597535.

[30] Adeyosfi MM and Harris A. Bayesian Theorem Application to Model Reservoir Facies Distribution on Deltaic Depositional Environment, Case Study of Browse Basin. In *Journal of Physics: Conference Series*. 2021; **2019**(1): 012083. DOI: https://doi.org/10.1088/1742-6596/2019/1/012083.